Additive Manufacturing of Ti_3C_2-MXene-Functionalized Conductive Polymer Hydrogels for ElectromagneticInterference Shielding

Ji Liu, Lorcan Mckeon, James Garcia, Sergio Pinilla, Sebastian Barwich, Matthias Möbius, Plamen Stamenov, Jonathan N. Coleman, and Valeria Nicolosi**

The ongoing miniaturization of devices and development of wireless and implantable technologies demand electromagnetic interference (EMI)shielding materials with customizability. Additive manufacturing of conductive polymer hydrogels with favorable conductivity and biocompatibility can offer new opportunities for EMI-shielding applications. However, simultaneously achieving high conductivity, design freedom, and shape fidelity in 3D printing of conductive polymer hydrogels is still very challenging. Here, an aqueous Ti_3C_2-MXene-functionalized poly(3,4-ethylenedioxythiophene):polystyrene sulfonate ink is developed for extrusion printing to create 3D objects with arbitrary geometries, and a freeze–thawing protocol is proposed to transform the printed objects directly into highly conductive and robust hydrogels with high shape fidelity on both the macro- and microscale. The as-obtained hydrogel exhibits a high conductivity of 1525.8 S m^{-1} at water content up to 96.6 wt% and also satisfactory mechanical properties with flexibility, stretchability, and fatigue resistance. Furthermore, the use of the printed hydrogel for customizable EMI-shielding applications is demonstrated. The proposed easy-to-manufacture approach, along with the highlighted superior properties, expands the potential of conductive polymer hydrogels in future customizable applications and represents a real breakthrough from the current state of the art.

J. Liu, L. Mckeon, J. Garcia, S. Pinilla, P. Stamenov, J. N. Coleman, V. Nicolosi
Centre for Research on Adaptive Nanostructures and Nanodevices (CRANN) and Advanced Materials Bio-Engineering Research Centre (AMBER)
Trinity College Dublin
Dublin 2, Dublin D02 PN40, Ireland
E-mail: ji.liu@tcd.ie; nicolov@tcd.ie
J. Liu, L. Mckeon, S. Pinilla, V. Nicolosi
School of Chemistry
Trinity College Dublin
Dublin 2, Dublin D02 PN40, Ireland
J. Liu, L. Mckeon, V. Nicolosi
I-FORM Advanced Manufacturing Research Centre
Trinity College Dublin
Dublin 2, Dublin D02 PN40, Ireland
J. Garcia, S. Barwich, M. Möbius, P. Stamenov, J. N. Coleman
School of Physics
Trinity College Dublin
Dublin 2, Dublin D02 PN40, Ireland

1. Introduction

The electromagnetic interference (EMI) shielding technique, based on applying a conductive barrier to cover the device and shield the electromagnetic field, is a viable approach to protect health and other sensitive devices from interference.[1,2] To this day, tremendous efforts have been made to achieve high shielding efficiency (SE) and multifunctionality by enhancing the electrical conductivity and optimizing the composition and structure of shielding materials.[3–10] However, high application flexibility, adaptability, and customizability are still required for shielding materials to meet the stringent requirements of next-generation applications, especially in situations where miniaturization is required.[11,12] Conventional shielding materials, such as metal foils, provide superb shielding efficiency but very limited customizability due to poor processability.[2,13] Moreover, with the development of wearable and implantable devices, shielding materials fabricated with bio-compatible materials are highly needed and would open up new opportunities for facilitating bioelectronic applications.[14,15]

Conductive hydrogel made from poly(3,4-ethylenedioxy thiophene):polystyrene sulfonate (PEDOT:PSS), one of the most promising conductive polymers, holds great potential for enabling new EMI-shielding applications due to the intrinsic electrical conductivity and biocompatibility as well as the favorable tissue-like mechanical properties and durability derived from the polymeric nature.[16] Unfortunately, the current fabrication of PEDOT:PSS hydrogels still mainly relies on conventional manufacturing strategies. Until now, only a few pioneering strategies have been demonstrated to shape/pattern PEDOT:PSS hydrogels: a molding approach in which the gelation of PEDOT:PSS dispersion is induced,[17,18] an electrochemical method based on the ionically induced cross-linking mechanism,[19] and a 3D-printing method in which the concentrated PEDOT:PSS dispersion is printed followed by repeated annealing and subsequent swelling process to transform the as-formed 2D patterns into 3D conductive hydrogels.[16,20] However, these cases have offered limited controllability on precisely forming PEDOT:PSS hydrogels with high conductivity and complex structures on 3D scales, limiting their customizable applications. To this day, precise

fabrication of highly conductive and robust PEDOT:PSS hydrogels with high design freedom and shape fidelity by 3D printing is still very challenging and largely unexplored. Besides, the shortcoming of the PEDOT:PSS hydrogels exists for shielding applications because of the limited conductivity at low solid content, and the posttreatments that are required for restoring the high conductivity derived from PEDOT could lead to collapse or severe deformation of the as-formed 3D architectures, affecting the printing shape fidelity.[17,20]

Here, we develop an aqueous Ti_3C_2-MXene-functionalized PEDOT:PSS ink with excellent 3D printability and leverage a freeze–thawing protocol to transform the printed architectures directly into highly conductive and robust hydrogels with high shape fidelity on both the macro- and microscale, offering a facile and highly reproducible route for additive manufacturing of conductive polymer hydrogels. The hydrophilic Ti_3C_2 MXene not only serves as an ink modifier to significantly improve the rheology properties of aqueous PEDOT:PSS ink for 3D printing without needing organic solvents but can also enhance the conductivity of the hydrogel. The 3D-printed hydrogel exhibits an unprecedented conductivity of 1525.8 S m^{-1} at a water content up to 96.6 wt%, outstanding durability, and also satisfactory mechanical properties with flexibility, stretchability, and fatigue resistance. We further demonstrate the concept of additive manufacturing-enabled customizable EMI shielding and reveal that the porous structure combined with the water-rich environment in the highly conductive hydrogel can greatly contribute to the ultimate EMI-shielding efficiency (EMI SE), ensuring excellent gigahertz shielding performance.

2. Results and Discussion

The 3D printable aqueous ink was prepared by dispersing the freeze-dried PEDOT:PSS into the MXene suspension synthesized by the chemical etching method (**Figure 1**a).[21] The ink was termed M_m-P_n, where *m* and *n* represent the concentration (mg in 0.1 mL H_2O) of MXene and PEDOT:PSS in the ink, respectively. Previously, it has been demonstrated that excellent extrusion printability of PEDOT:PSS ink can be achieved at low solid concentrations of ≥5 wt% by dissolving PEDOT:PSS into a binary solvent system (water/dimethyl sulfoxide) to form a reversible physical network.[20] Inspired by this, herein, we demonstrate that the rheological properties of the PEDOT:PSS solution can be easily improved by using a hydrophilic 2D material (Ti_3C_2 MXene) as an ink modifier, enabling the formation of a fully aqueous ink for extrusion printing and the enhancement of conductivity of the 3D-printed hydrogels.[22] Ti_3C_2 MXene is a newly emerged 2D transition metal carbide, which can simultaneously possess metallic conductivity and hydrophilicity owing to the surface terminations (mainly □OH and □F), showing excellent solution processibility and EMI-shielding performance.[1,10] The rich surface chemistry and rigid feature of MXene nanosheets ensure the interactions with PEDOT:PSS (Figure 1a) to facilitate the redispersion of PEDOT:PSS and the modification of the ink properties (viscosity, moduli, and shear yield stress),[22,23] which were confirmed by the rheological measurements (Figure 1b,d–g and Figures S1 and S2, Supporting Information). Owing to the synergy of MXene and PEDOT:PSS, excellent printability of the aqueous ink was easily achieved at a low solid concentration of ≥5 wt% (4 wt% PEDOT:PSS and 1 wt% MXene). The M1-P4 ink exhibits a distinct shear thinning behavior and a yield stress of ≈398 Pa, which is much higher than the basic requirement for 3D printing (Figure 1d–f).[24] The shear yield stress goes to ≈597 Pa for M1-P7 ink by increasing the PEDOT concentration (Figure 1f). Note that changing the MXene concentration can also tune the rheological properties. Benefiting from the favorable rheological properties, complex architectures, even with overhanging structures, can be easily fabricated by direct ink writing, indicating the superior 3D printability of the aqueous ink (Figure 1c). After printing, the ink moduli can rapidly recover in the absence of shear, allowing the printed architecture to retain the geometrical feature and the integrated structure. Note that the ink was kept in a fridge at 4 °C before being used and has a long shelf life of more than 30 days (Figure S3, Supporting Information).

The as-printed object can retain structural integrity without noticeable deformation after freeze-drying but can be further redispersed in water by vigorous vibration, indicating the weak cross-linking structure based on reversible physical bonds in the ink system (Figure 1h and Figure S4, Supporting Information). Scanning electron microscopy (SEM) imaging revealed that the as-printed filaments are highly porous with an open structure (Figure 1i). Note that inks with higher viscosity and higher yield stress are suitable for printing overhanging structures with wide spans, whereas the filaments printed by ink with lower viscosity and lower yield stress tend to partially merge, enabling the generation of more continuous structures, such as printed hydrogel meshes and films (Figure 1j,k).[12] Nevertheless, the as-printed filaments possess extremely poor structural robustness and low electrical conductivity of ≈25.8 S m^{-1} (M1-P4 ink) because of the weak cross-linking interactions between building blocks and the existence of excess insulating PSS component.[17] Thus, proper treatments should be applied to remove the PSS components and improve the structural integrity of the printed devices, ensuring favorable conductivity and mechanical performances, which are prerequisites for practical applications. Although excellent progress has been made in achieving outstanding conductive and mechanical properties of printed PEDOT:PSS hydrogels by controlled dry-annealing and rehydration,[16,20] an alternative method is still needed to allow the direct and precise transformation of the printed PEDOT:PSS devices into highly conductive and robust hydrogels without changing the printed structure during the post-treatment process, ensuring high shape fidelity.

Using H_2SO_4 treatment, which can efficiently dissolve the excessive PSS and increase the crystallinity of PEDOT without requiring a post-annealing process, has been proven to be one of the most effective ways for enhancing the structural integrity and conductivity of PEDOT:PSS materials.[17,25] However, typically, direct H_2SO_4 treatment would induce large volume contraction of porous PEDOT:PSS materials even when using a complicated method by gradually increasing the acid concentration,[17] severely affecting the shape accuracy for printing applications. Herein, with a freeze–thawing protocol, the

Figure 1. Design of 3D printable inks. a) Scheme illustrating the preparation of MXene-functionalized PEDOT:PSS ink for extrusion printing. b) Photographs of pristine PEDOT:PSS inks and MXene-functionalized PEDOT:PSS inks. c) Photographs of printed architectures. d) Viscosity versus shear rate, e) elastic modulus (*G′*) versus shear stress, f) shear yield stress, and g) frequency dependency of the ratio of *G′* and viscous modulus (*G″*) for different inks. h) Photographs showing the printed microlattice structure before and after freeze-drying. i–k) SEM images of freeze-dried printed devices. Scale

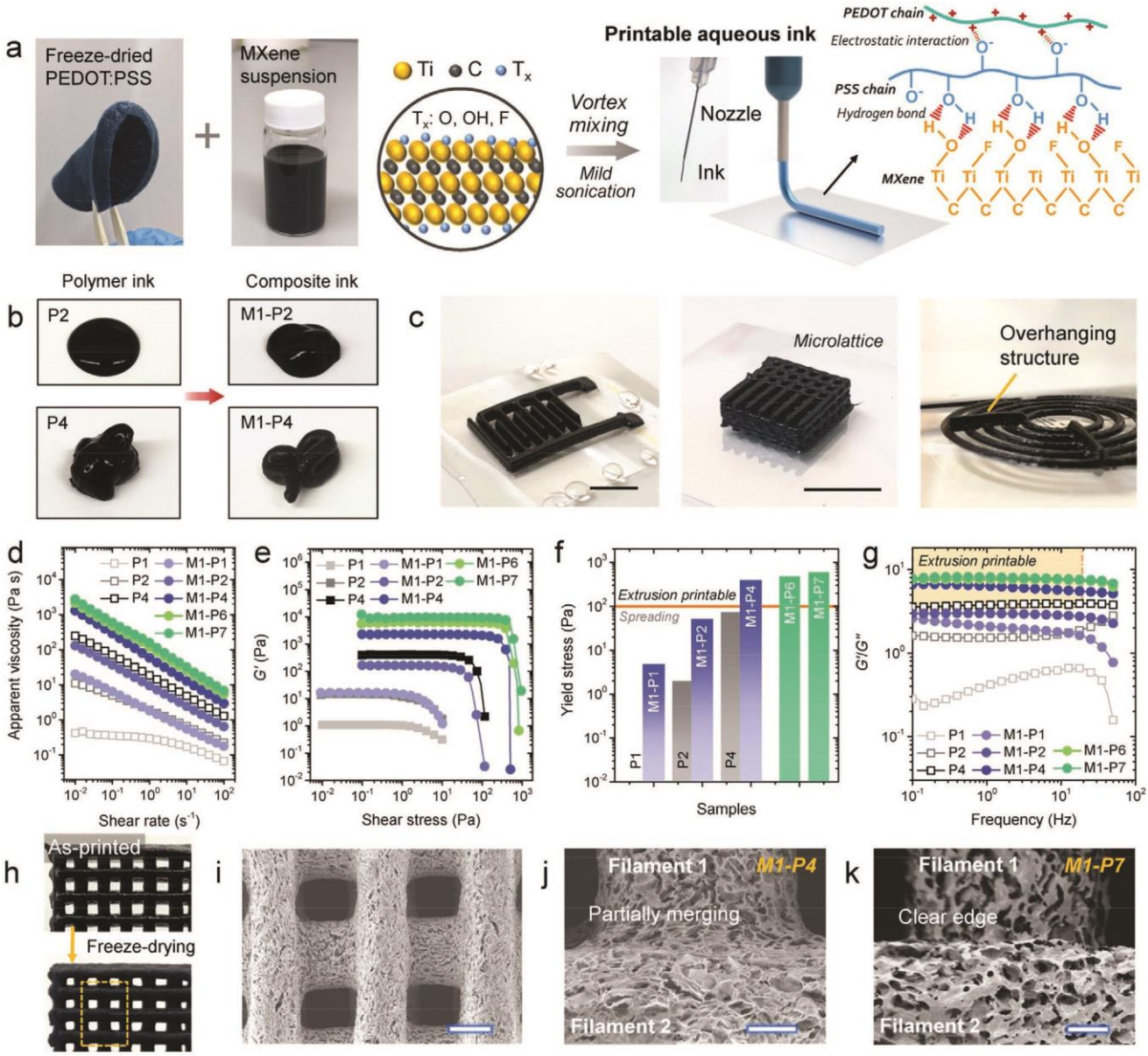

bars: c) 5 mm, i) 500 μm, j,k) 200 μm.

preliminary solidification of the as-printed architectures was exploited before high-concentration H_2SO_4 treatment to achieve spatial control and high shape fidelity. The typical procedures are as follows: first, the as-printed object was frozen in a −20 °C fridge, ensuring the formation of a skeleton structure, in which the network composed of PEDOT:PSS and MXene was fixed by the ice crystals. Then the frozen object was thawed in a 5 m H_2SO_4 solution at room temperature, which can initially induce a mild gelation and stabilize the as-formed structure (Figure S5, Supporting Information). Finally, the hydrogel was treated with high-concentration H_2SO_4 to dissolve excess PSS and expands the coils of PEDOT chains to further facilitate the gelation and enhance the electrical conductivity. As a result, the printed objects were directly converted into integrated hydrogels and their macroscopic shapes and sizes can be well retained due to the pre-solidification effect (**Figure 2**a–e and Figure S6, Supporting In formation). Figure 2e shows that the structural feature of a hydrogel device with a size of only a few millimeters was successfully retained after the freeze–thawing process followed by a high-concentration H_2SO_4 treatment. The SEM images further confirmed that the microscopic structures of the printed devices were not significantly affected

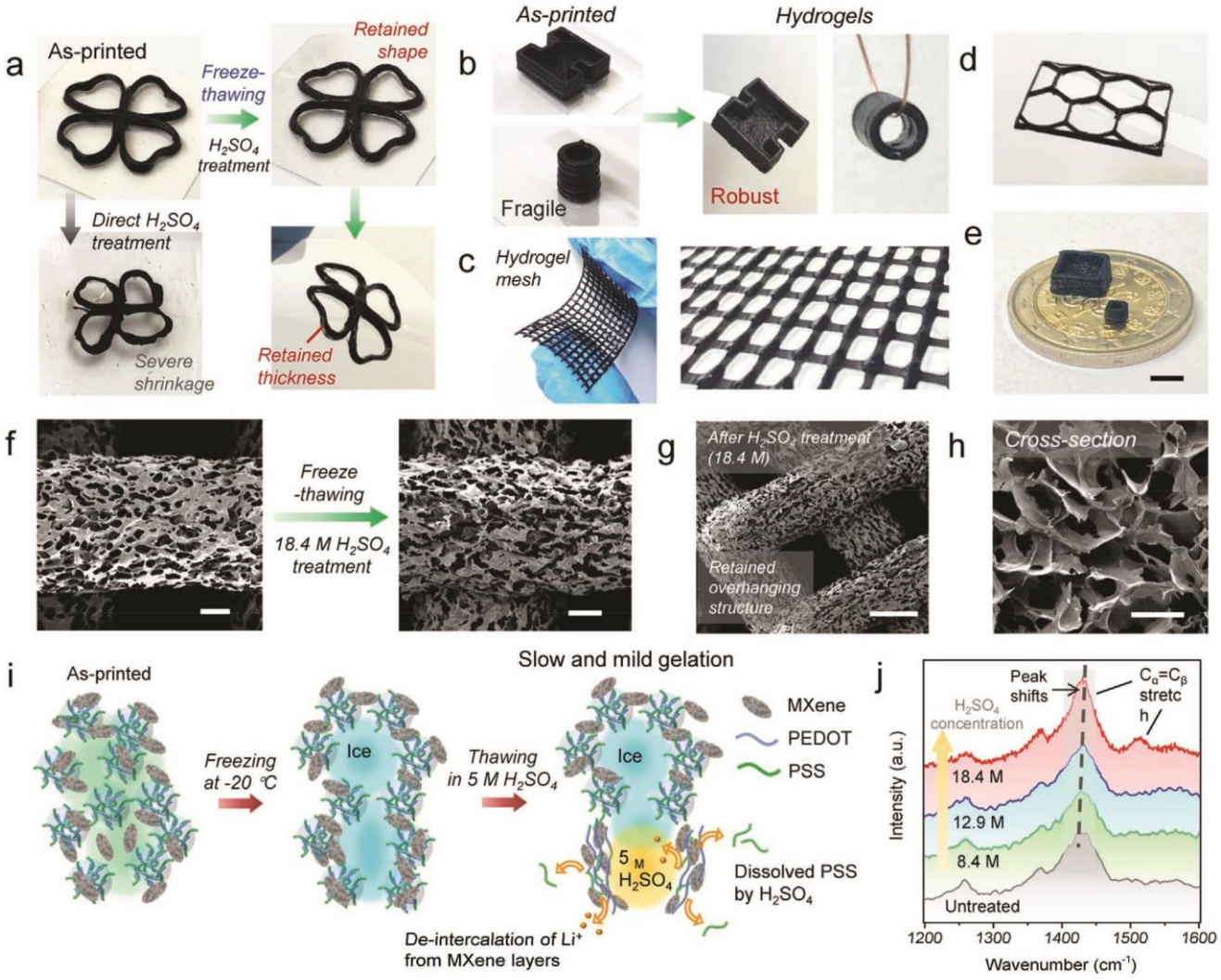

Figure 2. Post-treatment for generating hydrogels without affecting as-printed geometries. a,b) Photographs of the as-printed architectures before and after different post-treatments. c–e) Printed hydrogel samples obtained by freeze–thawing and 18.4 m H_2SO_4 treatments. f) SEM images of the printed filament before and after the freeze–thawing and 18.4 m H_2SO_4 treatments. g,h) SEM images of the printed hydrogel samples, showing that the microstructure is well retained after freeze–thawing and 18.4 m H_2SO_4 treatment. i) Schematic illustrating the mechanism of the freeze–thawing procedure. j) Raman spectra of the hydrogels treated with H_2SO_4 at different concentrations. Scale bars: e) 5 mm, f) 200 µm, g) 500 µm, h) 100 µm.

after the post-treatment, and only a tiny volume change was observed, depending on the H_2SO_4 concentration (Figure 2f–h and Figure S7, Supporting Information). After the post-treatment, the structural robustness of the hydrogel was also greatly enhanced (Figure 2b and Figures S8 and S9, Supporting Information). In striking contrast, the hydrogel obtained by direct H_2SO_4 treatment shows severe volume shrinkage and deformation (Figure 2a and Figure S10, Supporting Information). It is worth noticing that the freeze–thawing strategy is also effective for pure PEDOT:PSS samples, ensuring the precise fabrication of pure PEDOT:PSS hydrogels (Figure S11, Supporting Information).

As illustrated in Figure 2i, a possible mechanism is proposed for the freeze–thawing strategy. A freezing process at −20 °C is first applied to allow the slow formation of ice in the printed object, which can induce closer packing of MXene and PEDOT:PSS at the boundaries of ice crystals to form a skeleton structure,[26] as confirmed by the SEM image (Figure 1i). Then, during the thawing process, the ice melting begins from the outside end of the channel and the H_2SO_4 would slowly diffuse into the frozen objects, avoiding drastic reaction that may lead to severe volume shrinkage and deformation. To ensure successful diffusion of the acid into the porous structure for efficient pre-solidification, 5 m H_2SO_4 is selected for the thawing process due to the proper freezing point (Figure S12, Supporting Information). The low-concentration H_2SO_4 can preliminarily induce the conformational change of PEDOT chains and slightly dissolve PSS, ensuring an enhancement in structural robustness by mild gelation, which is key to reducing the shrinkage of the hydrogel in the followed procedure. Meanwhile, the H_2SO_4 as a protic acid is supposed to induce the deintercalation of Li^+ between MXene sheets, preventing the intercalation of H_2O between MXene sheets and thus facilitating the gelation.[27] Besides, the interactions between the PEDOT:PSS and MXene can also help resist the swelling effect and ensure less shape deformation.[28] Finally, the high-concentration H_2SO_4 treatment

further increases the crystallinity of PEDOT and removes excessive PSS component to restore the interchain π-stacking interaction between PEDOT, achieving stronger interfacial interactions and efficient electron transfer pathways, as evidenced by UV and Raman results (Figure 2j and Figures S13–S15, Supporting Information).[29,30] Note that, the H_2SO_4 is a nonsolvent of MXene and would not significantly affect the conductivity of MXene sheets (Figure S16, Supporting Information). In addition, it has been reported that the interaction between MXene and PEDOT:PSS can induce a doping effect for facilitating the phase transition of PEDOT:PSS, leading to an improvement of the conductive properties.[31] Thus, the high spatial controllability realized by the freeze– thawing strategy makes it feasible to precisely generate highly conductive and robust hydrogels with pre-designed geometries by 3D printing. Note that, some other mineral acids, such as HCl, can also enable the direct and precise conversion of the printed PEDOT:PSS-based devices into conductive and robust hydrogels through the freeze–thawing treatment (Figure S17, Supporting Information).

Having the typical printing and post-treatment protocols established, 3D-printed hydrogel films were fabricated for evaluating the conductive, mechanical, and EMI-shielding properties. Using extrusion printing, hydrogel films with tunable thickness can be easily fabricated, which can possess excellent flexibility even at a large thickness of more than 600 μm, further indicating the enhanced interfacial interactions among the components after H_2SO_4 treatment (**Figure 3**a). The electrical conductivity of the as-obtained hydrogel increased with the H_2SO_4 concentration. A high conductivity of ≈1525.8 S m^{-1} was achieved at a low solid content of ≈3.4 wt% for hydrogel printed with M1-P4 ink when freeze–thawing and 18.4 m H_2SO_4 treatments were applied (Figure 3b and Table S1, Supporting Information). Without adding MXene, the pure PEDOT:PSS hydrogel had a much lower conductivity of 660.9 S m^{-1}, similar to previous results,[17] indicating that not only the MXene sheets can modify the ink rheology but also largely contribute to the conductivity of the resulting hydrogel. Note that the hydrogel obtained by direct H_2SO_4 treatment showed a higher conductivity of ≈5517.2 S m^{-1} but a much higher solid content of 11.1 wt% arisen from the severe volume shrinkage (Figure S18, Supporting Information).

Interestingly, the deposition method of the ink can also be adapted to tune the microstructure and thus the properties of the hydrogel. The hydrogel film fabricated by extrusion printing showed an open and isotropic porous structure, whereas the hydrogel film fabricated by blade coating exhibited a highly oriented porous structure with compact surface morphology (Figure 3a). Note that, without adding MXene sheets, the blade-coated pure PEDOT:PSS hydrogel film showed a highly open porous structure, in which no significant orientation and compact surface were observed (Figure S19, Supporting Information). Thus, it is believed that the existence of 2D MXene sheets with high aspect ratio can also induce the orientation of the components in the hydrogel during the blade coating process.[32] The blade-coated hydrogel film with the unique oriented structure delivered an unprecedented conductivity of 5792.0 S m^{-1} at a low solid content of ≈4.2 wt% as well as excellent foldability, which is ranked at the top of the comparison chart when compared with previously reported conductive polymer hydrogels (Figure 3b and Table S1, Supporting Information). All these results indicate that the freeze–thawing process followed by high-concentration H_2SO_4 treatment can help achieve not only high printing shape fidelity by preventing the volume shrinkage of the printed hydrogel but also superb conductivity at high water content. Figure 3c shows that the printed hydrogel film served as a conductor to light up a light-emitting diode (LED) bulb under a low voltage of 3 V, confirming the high conductivity. More interestingly, even being repeatedly cut by a blade, the brightness of the bulb was not affected because of the viscoelasticity and the continuous highly conductive network of the hydrogel (Video S1, Supporting Information).[33]

The mechanical properties of the hydrogels were systematically investigated by applying tensile and compressive tests. For hydrogels fabricated with M1-P4 ink, both the ultimate tensile stress, Young's modulus, and maximum strain slightly increased as compared with those of pure PEDOT:PSS hydrogel (Figure 3d and Table S2, Supporting Information), indicating that the doping effect of MXene can also slightly strengthen the hydrogel by the interactions with PEDOT:PSS.[1,31] Note that further increasing the MXene content (M3-P4 ink) can enhance the conductivity but would lead to a significant deterioration in mechanical performance, owing to the lack of stretchability and limited gelation capability of MXene.[23,34] The printed hydrogel is also elastic, showing reversible stretchability/compressibility (Figure 3e and Figure S20, Supporting Information). It can recover to the original shape without breakage and significant plastic deformation even after being stretched to a tensile strain of 5%, indicating the enhanced cross-linking structure in the hydrogel and the improved structural integrity after the posttreatment (Figure 3e). Figure 3f shows the cyclic tensile curves. After the fatigue test of more than 100 cycles at a strain of 5%, the hydrogel still kept intact. The combination of moderate tensile strain, porous structure with thin cellular walls, and viscoelastic feature further endows the hydrogel with bending and even folding capability,[35] and the hydrogel shows small changes in electrical resistance upon deformation (Figure S21, Supporting Information). As shown in Figure 3g, even after 10 000 times of repeated bending at 90°, the conductivity of the hydrogel film can be retained with a relatively small resistance increment of 21.1%. Additionally, the hydrogel can keep the original shape without swelling over a long time of being immersed in water, further demonstrating its favorable long-term durability (Figure 3h).

The highly conductive and robust MXene-functionalized PEDOT:PSS hydrogels, fabricated by the precise and highly reproducible 3D printing technique, can be designed to possess arbitrary geometries and sizes to provide customizable EMIshielding solutions. The EMI SE of the printed hydrogels was measured to evaluate its ability for EMI shielding. Typically, the EMI SE is mainly determined by the conductivity and thickness of the shielding material.[1] The conductivity of the hydrogel increased with the H_2SO_4 concentration and the EMI SE follows the same trend. A high EMI SE of 51.7 dB was achieved at a hydrogel thickness of ≈295 μm (Figure 3i), indicating that more than 99.999% of the incident radiation was absorbed or reflected. This value is lower than some solid inorganic

Figure 3. Conductive, mechanical, and EMI-shielding properties. a) Photographs and SEM images of hydrogel films fabricated by different deposition methods. b) Comparison of the electrical conductivity as a function of solid content (details in Table S1, Supporting Information). c) Photographs of a hydrogel film as a conductor to light up an LED bulb at a voltage of 3 V. The hydrogel also shows autonomic self-healing performance. d) Typical tensile stress–strain curves. e) Stress–strain curve of the printed hydrogel at strains from 1% to 5%. f) The tensile stress–strain curves of the printed hydrogel at a strain of 5% for more than 100 cycles. g) Electrical resistance variations as a function of bending cycles (90°). h) Structural stability of the printed hydrogel in water. i) EMI SE curves in the frequency range of 8–12 GHz (X band). j) Simulated and experimental EMI SE of hydrogel and corresponding foam sample. k) Scheme of shielding mechanism. l) Photographs showing that the hydrogel can be printed to possess complex geometry

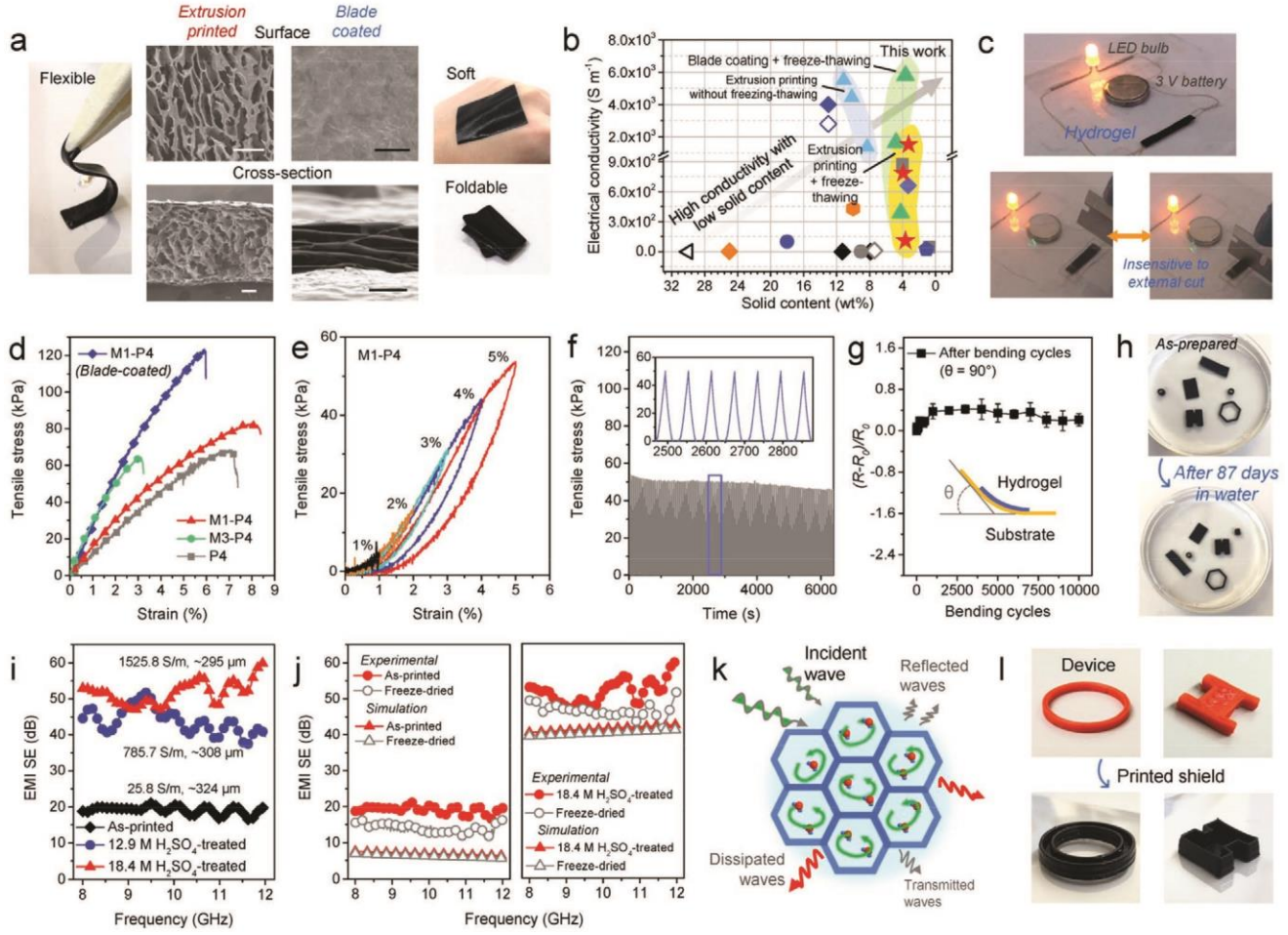

to perfectly fit the target device. Scale bars: 100 μm.

EMI-shielding materials, such as pure MXene films,[1] however, it is higher than that of most reported state-of-the-art polymer-based shielding materials (Table S3, Supporting Information),[36,37] satisfying the commercial requirements (computer: >15 dB, electronic control unit: >40 dB, sensor: >50 dB) (Figure S22, Supporting Information). Unexpectedly, the asprinted M1-P4 sample with an extremely low conductivity of ≈25.8 S m^{-1} and an electrically thin thickness of 324 μm (<skin depth) (Figure S23, Supporting Information) still exhibited a moderate EMI SE of ≈19.1 dB (Figure 3i).

To explore the unusual EMI-shielding mechanism, the theoretical EMI SE was calculated with Simon's formulism as follows[38]

$$\text{EMI SE} = 50 + 10\log\left(\frac{\sigma_f}{f}\right) + 1.7 d \sigma f \quad (1)$$

where σ, f, and d are the electrical conductivity (S cm^{-1}), frequency (MHz), and the thickness of the shield (cm), respectively. Note that the Simon's formulism only considers the conductive-property-related reflection (SE_R) and absorption (SE_A) parts, whereas other possible shielding mechanisms, such as internal multiple reflection and scattering, can also largely contribute to the ultimate EMI SE.[39] Figure 3j shows the comparison of experimental and theoretical EMI SE curves for the hydrogel samples and their corresponding freeze-dried foam samples. The experimental results of both as-printed and H_2SO_4-treated foam samples show discrepancy when compared with theoretical prediction, which should be attributed to the contributions from multireflection and scattering within the porous structure and the dipolar polarization of MXene.[4,40] For the hydrogel samples, the measured EMI SE is further higher than that of the foam samples. To further ascertain the shielding mechanism, the experimental SE_R, and SE_A were calculated, as shown in Figure S24, Supporting Information. The hydrogel samples have higher SE_A but similar SE_R when compared with the foam samples,

indicating that the enhancement of EMI SE is attributed to the absorption of the penetrated wave.[39] All these results imply that the porous structure combined with the internal water environment in the hydrogel is responsible for greatly improving EMI-shielding performance by contributing more absorption (Figure 3k).[41]

With the increasing proliferation of portable electronics and the trend toward miniaturization, EMI-shielding materials as a critical component in electronic devices also meet great challenges from the miniaturization aspect. Although great efforts have been made to provide ultrathin and multifunctional EMIshielding solutions,[10,11] fabrication strategy of EMI-shielding material with high design freedom on 3D scales is still sorely needed to improve the application adaptability and provide component-level EMI shielding. Here, we demonstrate that highly conductive and robust MXene-functionalized PEDOT:PSS hydrogels can be precisely and reproducibly fabricated to possess arbitrary geometries/sizes by 3D printing, which would allow the users to facilely create customizable and conformal EMI-shielding solutions that precisely meet their real needs with minimum material waste and prototyping cost. As a demonstration, we printed hydrogel EMI-shielding materials with predesigned geometries for perfectly conforming the device geometry and meeting the precise shielding requirements (Figure 3l). Furthermore, these hydrogels can be easily converted into foam materials by freeze-drying, enabling an accessible way to produce lightweight EMI-shielding materials by 3D printing for various application scenarios (Figure S25, Supporting Information). Therefore, the conductive polymer-based hydrogels fabricated by additive manufacturing can offer new opportunities for EMIshielding applications in situations where external EMI should be shielded for the safe operation of sensitive components, where space is limited, and where biocompatibility of materials is required, such as implants and microelectronic systems.

3. Conclusion

We have demonstrated the precise fabrication of Ti_3C_2-MXenefunctionalized PEDOT:PSS hydrogels by 3D printing. A highly printable aqueous ink is developed by using MXene to modify the PEDOT:PSS ink rheology and a freeze–thawing protocol is proposed to transform the printed objects directly into highly conductive and robust hydrogels with high shape fidelity on both macro- and microscales. The as-obtained hydrogel shows ultrahigh conductivity, outstanding durability, and good mechanical properties with even reversible stretchability and compressibility at extremely high water content. Furthermore, the combination of high conductivity, porous structure, and internal water environment endows the hydrogel with outstanding EMI-shielding performance at small thickness, and its printable feature promises customizable applications for satisfying the trend in the miniaturization of electronic devices. We foresee that, these highly conductive hydrogels with open porous structure, fabricated by additive manufacturing technique, also hold great potential in the fields of energy storage, water desalination, and wearable and implantable electronics.

Acknowledgements

The authors thank the Advanced Microscopy Laboratory for the provision of their facilities and Carbon-Ukraine and Prof. Yury Gogotsi for providing the Ti_3AlC_2 MAX phase. This publication has emanated from research supported in part by a research grant from Science Foundation Ireland (SFI) AMBER (12/RC/2278_P2), co-funded under the European Research Council (ERC) CoG 3D2Dprint (GA 681544) and PoC Powering_eTextiles (GA 861673). L.M. acknowledges support from SFI I-Form centre. S.P. was supported by European Union's Horizon 2020 research and innovation programme under the Marie Skłodowska-Curie grant agreement (713567). M.M. acknowledges support from SFI, grant number SFI 17/CDA/4704.

Conflict of Interest

The authors declare no conflict of interest.

Data Availability Statement

The data that support the findings of this study are available from the corresponding author upon reasonable request.

Keywords

additive manufacturing, electromagnetic-interference shielding, hydrogels, MXenes, poly(3,4-ethylenedioxythiophene):polystyrene sulfonate (PEDOT:PSS)

[1] F. Shahzad, M. Alhabeb, C. B. Hatter, B. Anasori, S. Man Hong, C. M. Koo, Y. Gogotsi, *Science* **2016**, *353*, 1137.

[2] Q. Wei, S. Pei, X. Qian, H. Liu, Z. Liu, W. Zhang, T. Zhou, Z. Zhang, X. Zhang, H.-M. Cheng, W. Ren, *Adv. Mater.* **2020**, *32*, 1907411.

[3] S. Wan, Y. Chen, S. Fang, S. Wang, Z. Xu, L. Jiang, R. H. Baughman, Q. Cheng, *Nat. Mater.* **2021**, *20*, 624.

[4] J. Liu, H.-B. Zhang, R. Sun, Y. Liu, Z. Liu, A. Zhou, Z.-Z. Yu, *Adv. Mater.* **2017**, *29*, 1702367.

[5] Z. Zeng, F. Jiang, Y. Yue, D. Han, L. Lin, S. Zhao, Y.-B. Zhao, Z. Pan, C. Li, G. Nyström, J. Wang, *Adv. Mater.* **2020**, *32*, 1908496.

[6] B. Yao, W. Hong, T. Chen, Z. Han, X. Xu, R. Hu, J. Hao, C. Li, H. Li, S. E. Perini, M. T. Lanagan, S. Zhang, Q. Wang, H. Wang, *Adv. Mater.* **2020**, *32*, 1907499.

[7] B. Shen, W. Zhai, W. Zheng, *Adv. Funct. Mater.* **2014**, *24*, 4542.

[8] Q.-W. Wang, H.-B. Zhang, J. Liu, S. Zhao, X. Xie, L. Liu, R. Yang, N. Koratkar, Z.-Z. Yu, *Adv. Funct. Mater.* **2019**, *29*, 1806819.

[9] L. Li, S. Zhao, X.-J. Luo, H.-B. Zhang, Z.-Z. Yu, *Carbon* **2021**, *175*, 594.

[10] W. Chen, L.-X. Liu, H.-B. Zhang, Z.-Z. Yu, *ACS Nano* **2021**, *15*, 7668.

[11] T. Yun, H. Kim, A. Iqbal, Y. S. Cho, G. S. Lee, M.-K. Kim, S. J. Kim, D. Kim, Y. Gogotsi, S. O. Kim, C. M. Koo, *Adv. Mater.* **2020**, *32*, 1906769.

[12] S. Zhao, G. Siqueira, S. Drdova, D. Norris, C. Ubert, A. Bonnin, S. Galmarini, M. Ganobjak, Z. Pan, S. Brunner, G. Nyström, J. Wang, M. M. Koebel, W. J. Malfait, *Nature* **2020**, *584*, 387.

[13] N. Li, Y. Huang, F. Du, X. He, X. Lin, H. Gao, Y. Ma, F. Li, Y. Chen, P. C. Eklund, *Nano Lett.* **2006**, *6*, 1141.

[14] S. M. Won, L. Cai, P. Gutruf, J. A. Rogers, *Nat. Biomed. Eng.* **2021**, https://doi.org/10.1038/s41551-021-00683-3.

[15] S. Choi, S. I. Han, D. Jung, H. J. Hwang, C. Lim, S. Bae, O. K. Park, C. M. Tschabrunn, M. Lee, S. Y. Bae, J. W. Yu, J. H. Ryu, S.-W. Lee, K. Park, P. M. Kang, W. B. Lee, R. Nezafat, T. Hyeon, D.-H. Kim, *Nat. Nanotechnol.* **2018**, *13*, 1048.

[16] B. Lu, H. Yuk, S. Lin, N. Jian, K. Qu, J. Xu, X. Zhao, *Nat. Commun.* **2019**, *10*, 1043.
[17] B. Yao, H. Wang, Q. Zhou, M. Wu, M. Zhang, C. Li, G. Shi, *Adv. Mater.* **2017**, *29*, 1700974.
[18] S. Zhang, Y. Chen, H. Liu, Z. Wang, H. Ling, C. Wang, J. Ni, B. Çelebi-Saltik, X. Wang, X. Meng, H.-J. Kim, A. Baidya, S. Ahadian, N. Ashammakhi, M. R. Dokmeci, J. Travas-Sejdic, A. Khademhosseini, *Adv. Mater.* **2020**, *32*, 1904752.
[19] V. R. Feig, H. Tran, M. Lee, K. Liu, Z. Huang, L. Beker, D. G. Mackanic, Z. Bao, *Adv. Mater.* **2019**, *31*, 1902869.
[20] H. Yuk, B. Lu, S. Lin, K. Qu, J. Xu, J. Luo, X. Zhao, *Nat. Commun.* **2020**, *11*, 1604.
[21] M. Alhabeb, K. Maleski, B. Anasori, P. Lelyukh, L. Clark, S. Sin, Y. Gogotsi, *Chem. Mater.* **2017**, *29*, 7633.
[22] B. Akuzum, K. Maleski, B. Anasori, P. Lelyukh, N. J. Alvarez, E. C. Kumbur, Y. Gogotsi, *ACS Nano* **2018**, *12*, 2685.
[23] S. Umrao, R. Tabassian, J. Kim, V. H. Nguyen, Q. Zhou, S. Nam, I.-K. Oh, *Sci. Rob.* **2019**, *4*, eaaw7797.
[24] C. B. Highley, K. H. Song, A. C. Daly, J. A. Burdick, *Adv. Sci.* **2019**, *6*, 1801076.
[25] Y. H. Kim, C. Sachse, M. L. Machala, C. May, L. Müller-Meskamp, K. Leo, *Adv. Funct. Mater.* **2011**, *21*, 1076.
[26] M. Hua, S. Wu, Y. Ma, Y. Zhao, Z. Chen, I. Frenkel, J. Strzalka, H. Zhou, X. Zhu, X. He, *Nature* **2021**, *590*, 594.
[27] H. Chen, H. Ma, P. Zhang, Y. Wen, L. Qu, C. Li, *ACS Nano* **2020**, *14*, 10471.
[28] X. Wu, T. Tu, Y. Dai, P. Tang, Y. Zhang, Z. Deng, L. Li, H.-B. Zhang, Z.-Z. Yu, *Nano-Micro Lett.* **2021**, *13*, 148.
[29] J. Ouyang, Q. Xu, C.-W. Chu, Y. Yang, G. Li, J. Shinar, *Polymer* **2004**, *45*, 8443.
[30] S. Garreau, G. Louarn, J. P. Buisson, G. Froyer, S. Lefrant, *Macromolecules* **1999**, *32*, 6807.
[31] G. S. Gund, J. H. Park, R. Harpalsinh, M. Kota, J. H. Shin, T.-i. Kim, Y. Gogotsi, H. S. Park, *Joule* **2019**, *3*, 164.
[32] J. Zhang, N. Kong, S. Uzun, A. Levitt, S. Seyedin, P. A. Lynch, S. Qin, M. Han, W. Yang, J. Liu, X. Wang, Y. Gogotsi, J. M. Razal, *Adv. Mater.* **2020**, *32*, 2001093.
[33] S. Zhang, F. Cicoira, *Adv. Mater.* **2017**, *29*, 1703098.
[34] Y. Deng, T. Shang, Z. Wu, Y. Tao, C. Luo, J. Liang, D. Han, R. Lyu, C. Qi, W. Lv, F. Kang, Q.-H. Yang, *Adv. Mater.* **2019**, *31*, 1902432.
[35] R. Huang, M. Huang, X. Li, F. An, N. Koratkar, Z.-Z. Yu, *Adv. Mater.* **2018**, *30*, 1707025.
[36] R. Sun, H.-B. Zhang, J. Liu, X. Xie, R. Yang, Y. Li, S. Hong, Z.-Z. Yu, *Adv. Funct. Mater.* **2017**, *27*, 1702807.
[37] H. Abbasi, M. Antunes, J. I. Velasco, *Prog. Mater. Sci.* **2019**, *103*, 319.
[38] R. M. Simon, *Polym.-Plast. Technol. Eng.* **1981**, *17*, 1.
[39] A. Iqbal, P. Sambyal, C. M. Koo, *Adv. Funct. Mater.* **2020**, *30*, 2000883.
[40] A. Iqbal, F. Shahzad, K. Hantanasirisakul, M.-K. Kim, J. Kwon, J. Hong, H. Kim, D. Kim, Y. Gogotsi, C. M. Koo, *Science* **2020**, *369*, 446.
[41] W.-L. Song, Y.-J. Zhang, K.-L. Zhang, K. Wang, L. Zhang, L.-L. Chen, Y. Huang, M. Chen, H. Lei, H. Chen, D. Fang, *Adv. Sci.* **2020**, *7*, 1902162.